Meteoric, marine and total ice thickness maps of Filchner-Ronne-Schelfeis, Antarctica

H. Sandhäger [1] , D.G. Vaughan [2], and A. Lambrecht [1]

[1] *Alfred-Wegener-Institut für Polar- und Meeresforschung, Postfach 120161, D-27515 Bremerhaven*
[2] *British Antarctic Survey, High Cross, Madingley Road, Cambridge CB3 0ET, UK*

Introduction

Mapping the geometry of the ice sheet is fundamental to many advanced investigations, e.g., on ice dynamics, mass balance, ice – ocean interaction, ice – atmosphere interaction, and ice body sensitivity to climate change. Regarding the Filchner-Ronne-Schelfeis (FRIS; Fig.1), several research institutes from different countries carried out extensive ice thickness measurements during various field campaigns. The individual data sets were used to compile diverse ice thickness maps and digital ice thickness models. However, most of these results include only sub-areas of FRIS (see references given in Table 1).

The aim of this combined analysis of all available source data sets is to derive a comprehensive ice thickness model for the entire FRIS. Besides the three main parts, which are the Ronne Ice Shelf in the west, the Filchner-Schelfeis in the east, and the ice rise Berkner Island in-between, several smaller ice rises and ice rumples have to be considered (Fig. 1). Since the mass discharge from inland into FRIS is concentrated on few glaciers and ice streams, a strongly differentiated and complex ice thickness distribution occurs particularly near the grounding lines. Hence, an adequate thickness model will only be obtained if the model grid resolution is sufficiently high. Another important glaciological feature of FRIS is a double-layer structure of large parts of the floating ice body. While the upper layer of

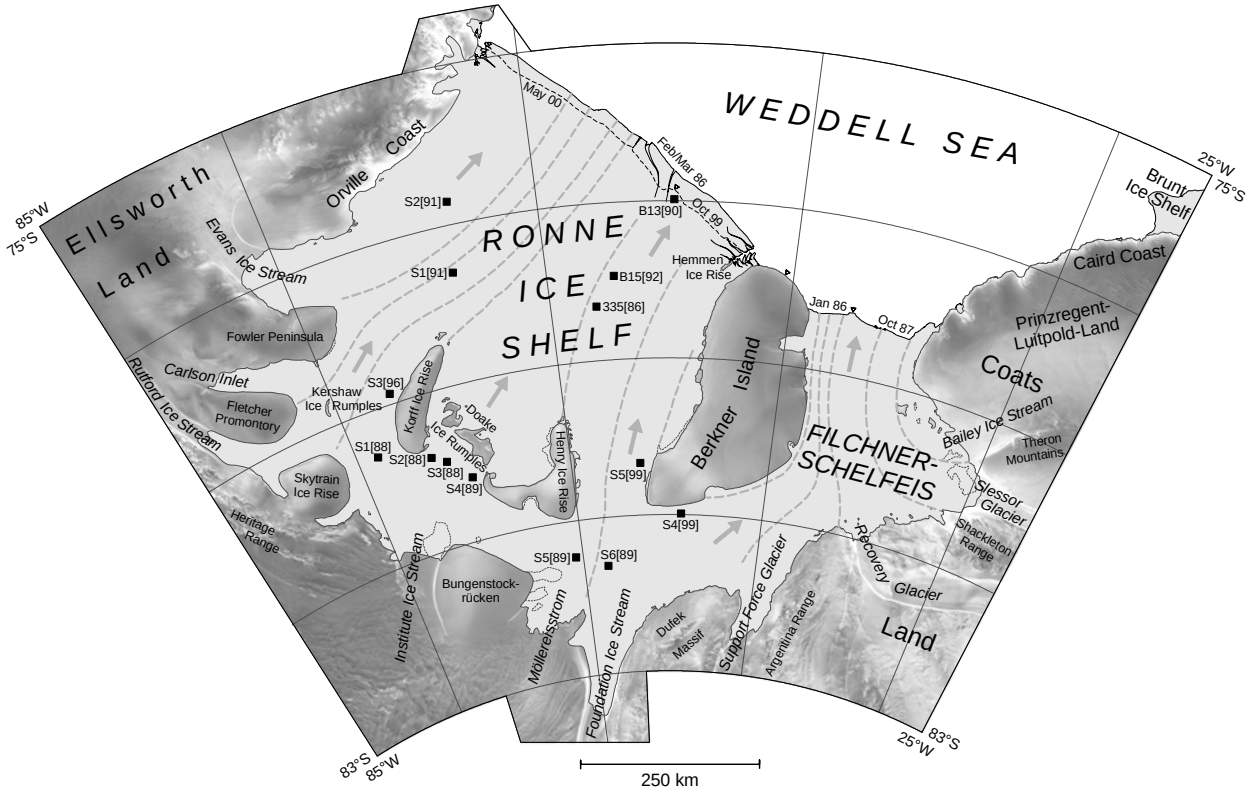

Figure 1: Map of FRIS and the adjacent inland ice. The RADARSAT SAR image mosaic of the grounded ice (Jezek and RAMP Product Team, 2002) clearly shows ice streams, glaciers, and mountainous regions. Arrows and selected flowlines (dashed light grey lines) indicate the basic structure of the ice shelf flow regime. The positional change of the Ronne Ice Shelf front between Feb. / Mar. 1986 and Oct. 1999 / May 2000 is partly due to the calving of icebergs A-38 to A-44. Grounding line, ice front, and flowline positions are adopted from Heidrich et al. (1992) and ADD Consortium (2002); the grounding line of Foundation Ice Stream is mapped according to Lambrecht (1998). The drill sites listed in Table 3 are marked by squares.

meteoric ice is formed due to snow accumulation, the formation process of the basal layer of marine ice results from crystallisation of ice platelets in the water column, buoyant agglomeration of these platelets at the ice shelf base, and eventually consolidation. The occurrence of the two types of ice requires a comprehensive thickness model to describe meteoric, marine, and total ice thickness distributions.

Ice thickness data base and subsidiary digital elevation model

Most of the basic ice thickness data sets of FRIS derive from radio-echo sounding (RES) surveys (Table 1). The RES technique is adequate for mapping meteoric ice thickness, because the absorption of radio wave energy is sufficiently low and both ice surface and bottom of the meteoric ice layer (interface between meteoric ice and sea water or marine ice) usually produce strong radar reflections. Compared to that, in marine ice the absorption is considerably higher and generally prevents large basal marine ice layers from being observed with RES. Furthermore, an effective bottom reflector is absent at least in the formation areas of marine ice, where rather a continuous transition from consolidated marine ice to unconsolidated ice platelets occurs ('slush-layer') than a definite marine ice / sea water interface. By incorporating three seismic reflection data sets of meteoric ice thickness to the RES data base, we obtained an acceptable data point coverage of FRIS apart from the Filchner-Schelfeis region (Fig. 2). The auxiliary data used to reduce the data gap derives from digitisation of an ice thickness map published by Pozdeev and Kurinin (1987) and transformation of ice shelf surface elevations to (meteoric) ice thicknesses (Table 1). This approach is only applicable to Filchner-Schelfeis sections supposed not to have a basal marine ice layer (cf., Grosfeld et al., 1998). The ice surface elevations have been extracted from the ESAMCA Digital Elevation Model (ESAMCA DEM; Sievers et al., 1995; Mantripp et al., 1996; Wingham et al., 1997) which is based on satellite altimetry data and describes the surface topography of large parts of FRIS in good planimetric detail. The vertical accuracy of the DEM is specified as ± 5 m. A regression of the relevant RES and seismic measurements against corresponding elevations from the ESAMCA DEM yields the required hydrostatic relation for ice shelf areas where only meteoric ice is expected:

$$(1) \quad H_{met} = 9.26\,(h - 15.5\ \mathrm{m} - \Delta h_2) = \frac{\rho_w}{\rho_w - \rho_c}(h - \Delta h_1 - \Delta h_2)$$

where H_{met} is the meteoric ice thickness, h is the surface elevation a.s.l., ρ_w and ρ_c are the densities of sea water and consolidated ice, and Δh_1 is a constant correction for firn layer density. The second correction Δh_2 considers discrepancies from the regression line $H_{met} = 9.26\,(h - 15.5\ \mathrm{m})$ due to incorrect

Source location	Data type	Date	Data points	
AWI, Bremerhaven, Germany	airborne RES	1994/95	22 060	(1)
AWI, Bremerhaven, Germany	seismic reflection	1995	106	(1)
BAS, Cambridge, UK	airborne RES	1974/75 - 1987/88	13 665	(2)
BAS, Cambridge, UK	seismic reflection	1994/95	131	(3)
DPG, Stockholm, Sweden	airborne RES	1991/92	19	(4)
IGM, Münster, Germany	airborne RES	1985/86, 1989/90	10 352	(5)
IGM, Münster, Germany	ground-based RES	1989/90	314	(6)
SG, St. Petersburg, Russia	seismic reflection	1976 -1986	308	(7)
SPRI, Cambridge, UK	airborne RES	1977/78, 1978/79	3 068	(2)
SG, St. Petersburg, Russia	digitised thickness contour lines	1987	413	(7)
ESAMCA Project	ERS-1 radar-altimeter data	1993	1 239	(8)

Table 1: Basic data sets used to derive the digital meteoric ice thickness model of FRIS. (*AWI*: Alfred-Wegener-Institut für Polar- und Meeresforschung; *BAS*: British Antarctic Survey; *DPG*: Department of Physical Geography and Quaternary Geology, Stockholm University; *IGM*: Institut für Geophysik der Universität Münster; *SG*: Sevmorgeologija of the Ministry of Geology (of the former USSR); *SPRI*: Scott Polar Research Institute, University of Cambridge; ESAMCA: Exploitation of satellite altimetry for the monitoring of climate-related change of Antarctic ice shelves) (Source data references: (1) Hempel and Oerter, 1995, Lambrecht et al., 1995, 1999, Lambrecht, 1998; (2) Robin et al., 1983, Crabtree and Doake, 1986, Vaughan et al., 1991; (3) Johnson and Smith, 1997; (4) Holmlund, 1992; (5) Thyssen, 1988, 1991, Thyssen et al., 1992, Grosfeld et al., 1998; (6) Blindow, 1994; (7) Pozdeev and Kurinin, 1987; (8) Sievers et al., 1995, Mantripp et al., 1996, Wingham et al., 1997)

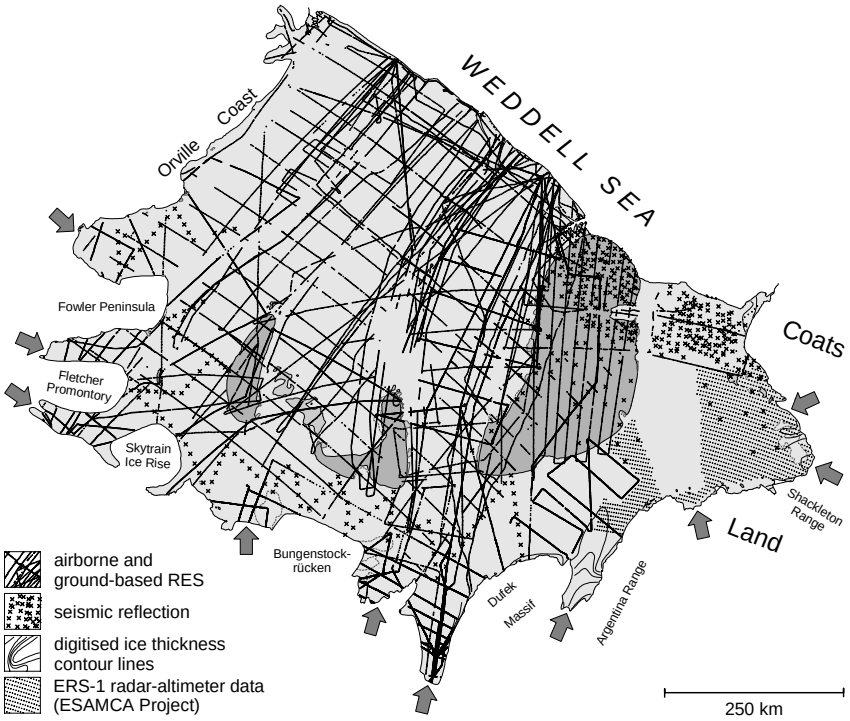

Figure 2: Distribution of the meteoric ice thickness measurements used to determine the digital thickness model of FRIS. The major part of the data base results from RES and seismic reflection surveys. A improvement of the data point coverage of the Filchner-Schelfeis region is attained by including two auxiliary data sets with digitised thickness contours and converted surface elevations, respectively (cf. Table 1). Arrows indicate entrances of main contributory glaciers and ice streams governing most of the mass discharge from inland into FRIS.

geometric data or locally modified glaciological conditions (e.g., occurrence of crevasses, stress-induced enhancement of firn densification, deviations from hydrostatic equilibrium near grounding lines). Although Δh_2 varies from several metres up to a few tens of metres, $\Delta h_2 \approx 0$ holds for most ice shelf areas. Provided that $\rho_w \approx 1028\,\mathrm{kg\,m^{-3}}$ is a reliable estimation for the density of the sea water beneath the ice shelf, Equation (1) involves an ice density $\rho_c \approx 917\,\mathrm{kg\,m^{-3}}$ close to that of solid ice.

Determination of the digital ice thickness model

The digital geometric model describing the meteoric ice thickness distribution of FRIS results from interpolation of the data base specified in Table 1 on a regular horizontal grid. After testing different interpolation algorithms, the final computation was performed with a geostatistical gridding method (Kriging) which attempts to express trends that are suggested in the source data. The chosen grid spacing of 1.67 km provides for an acceptable resolution of even comparatively small topographic features such as the Kershaw Ice Rumples ($\sim 80\,\mathrm{km^2}$) or the Hemmen Ice Rise ($\sim 75\,\mathrm{km^2}$), both located within the Ronne Ice Shelf (cf., Fig. 1). Due to the lack of meteoric ice thickness data from the central Filchner-Schelfeis (Fig. 2), no reliable gridding results were obtained for this region. Hence, it is marked as data gap in the gridded data set.

The thickness model for the basal marine ice of FRIS is determined from an expanded hydrostatic relation which incorporates the difference in meteoric and marine ice densities. By analysing the ice core obtained at drill site B15[1992] (Fig. 1), Oerter et al. (1992a) acquired a depth density profile comprising the double-layer structure of the ice shelf body in the central part of the Ronne Ice Shelf. They found the densities of consolidated meteoric and marine ice are $\rho_{c\,|\,met} = (896 \pm 9)\,\mathrm{kg\,m^{-3}}$ and $\rho_{c\,|\,mar} = (911 \pm 6)\,\mathrm{kg\,m^{-3}}$, respectively. This suggests that the hydrostatic relation (1) overestimates the mean density of consolidated ice in the FRIS region and, hence, cannot be directly adapted to ice shelf areas composed of two types of ice. Since Equation (1) results from a regression of ice thicknesses against surface elevations, both geometric data sets were scrutinised for possible erroneous offsets leading to the overestimation of the ice density. While the different data sets of meteoric ice thickness show an overall high consistency, a comparison between the ESAMCA DEM and a topographic map of FRIS compiled mainly from airborne altimetry and ground-based levelling data (Mantripp et al., 1996) reveals a significant mismatch particularly for the central Ronne Ice Shelf. Thus, we cannot be

sure that the ESAMCA DEM is not affected by a negative offset of several metres at least for this region. Assuming that (i) the surface elevations from the ESAMCA DEM are too low for all ice shelf areas with basal marine ice, (ii) the ice densities measured at drill site B15[1992] are representative for all these areas, and (iii) the marine ice is completely consolidated, an expanded hydrostatic relation for the double-layered ice shelf section of FRIS reads:

$$(2) \qquad H_{mar} = \frac{\rho_w}{\rho_w - \rho_{c|mar}} \left[a\,(h - \Delta h_1 - \Delta h_2) - \left(1 - \frac{\rho_{c|met}}{\rho_w}\right) H_{met} \right]$$

where H_{mar} is the marine ice thickness and a is a parameter compensating for the assumed erroneous elevation offset. A steady transition between Equations (1) and (2) is attained by specifying $a = 1.19$. In the strict sense, H_{mar} represents an 'equivalent' thickness of a single homogeneous marine ice layer causing the same buoyancy as a composition of upper consolidated ice and a lower slush-layer.
The distribution of the correction Δh_2 in ice shelf regions with basal marine ice is estimated by carefully extrapolating the known Δh_2 pattern of the other areas. However, only portions of Δh_2 related to locally modified glaciological conditions are considered. Using the ESAMCA DEM and the new gridded meteoric ice thickness data set, Equation (2) yields the thickness model describing the geometry of the marine ice layers beneath FRIS, except for the data gap in the Filchner-Schelfeis.

The digital geometric model for the total ice thickness distribution of FRIS directly results from adding the new gridded meteoric and marine ice thickness data sets. To estimate the total ice thickness distribution in the central Filchner-Schelfeis, Equation (1) was used to convert elevations from the ESAMCA DEM. Thus, the final total ice thickness model includes the entire FRIS region.

The accuracy of the new ice thickness model for FRIS depends on a number of individual errors. Of particular relevance are the errors in the different basic ice thickness data sets, in the ESAMCA DEM, due to the data gridding, and in defining the hydrostatic relation parameters. A corresponding estimation yields the probable error tolerances listed in Table 2.

A validation of the thickness model is performed by comparison with available borehole data (Table 3). The discrepancies between the ice thicknesses measured at the different drill sites and the respective values extracted from the new geometric model are smaller than the estimated error tolerances.

	H_{met}	H_{mar}	H_{tot}
Areas with many RES / seismic data points and small thickness gradients	± 25 m	± 70 m	± 25 m ($H_{mar} = 0$) ± 75 m ($H_{mar} > 0$)
Other areas	± 25 m to ± 200 m	± 70 m to ± 90 m	± 25 m to ± 200 m ($H_{mar} = 0$) ± 75 m to ± 105 m ($H_{mar} > 0$)

Table 2: Estimated error tolerances for the meteoric, marine, and total ice thicknesses in the new geometric model for FRIS.

Drill site	H_{met} (m)		H_{mar} (m)		Drill site	H_{met} (m)		H_{mar} (m)	
Site 1 [1988] (1)	1020	1041	0	0	335 [1986] (3)	170	166	260+35	262
Site 2 [1988] (1)	1005	993	0	0	B15 [1992] (4)	153	159	269	243
Site 3 [1988] (1)	995	996	0	0	Site 1 [1991] (5)	517	516	31+14	0
Site 4 [1989] (1)	975	952	0	0	Site 2 [1991] (6)	541	537	0	3
Site 5 [1989] (1)	990	981	0	0	Site 3 [1996] (7)	825	815	0	0
Site 6 [1989] (1)	1095	1108	0	0	Site 4 [1999] (8)	941	936	0	3
B13 [1990] (2)	153	163	86	57	Site 5 [1999] (8)	763	766	0	0

Table 3: Meteoric and marine ice thicknesses measured at 14 drill sites on FRIS and respective values from the new ice thickness model (light grey columns). At sites 335 [1986] and Site 1 [1991] the measurements provide distinction between upper consolidated marine ice and a lower slush-layer. Drill site locations are indicated in Figure 1. ((1) Vaughan, 1990; (2) Oerter et al., 1992b; (3) Engelhardt and Determann, 1986; (4) Oerter et al., 1992a; (5) Nicholls et al., 1991; (6) Robinson and Makinson, 1992; (7) Makinson, 1996; 8 Nicholls et al., 2001)

Ice thickness maps and integral quantities related to ice body geometry

The new digital geometric model was used to derive a series of detailed thematic maps showing the meteoric, marine and total ice thickness distributions of FRIS (Fig. 3 a, b, c). The largest meteoric ice thicknesses of more than 1500 m occur close to the grounding zones of the main contributory glaciers and ice streams. Since most of the mass discharge from inland into FRIS is concentrated on these drainage systems, they substantially influence the flow regime and the geometry of the ice shelf body. However, the geometric and dynamic characteristics of FRIS also depend on the distribution of ice rises, ice rumples, and prominent inland regions which cause restraint and/or deflection of the ice shelf flux. Such processes evidently contribute to the conspicuous thinning of the meteoric ice layer and the development of distinct basal marine ice bodies (Fig. 3 b). While the geometry of the marine ice layer beneath the Filchner-Schelfeis is still not well known, the new thickness model yields a comprehensive description of the three major marine ice bodies beneath the Ronne Ice Shelf. The largest one located in the central Ronne Ice Shelf reaches its maximum thickness of about 400 m to the north of Henry Ice Rise where the upper meteoric ice layer thins to less than 200 m.
Besides their typical elongated shapes resulting from advection with the ice shelf flow, the three marine ice bodies beneath the Ronne Ice Shelf are characterized by a continuous thinning with decreasing distance from the ice front. This is consistent with the expected situation that the accumulation rate of marine ice is highest beneath the southern (upstream) part of each marine body while further north (downstream) basal melt processes are dominating (cf., Bombosch and Jenkins, 1995). Due to this persistent erosion, the marine ice layers beneath the Ronne Ice Shelf do not extend up to the calving front. Thus, calving icebergs presumably comprise only little or no marine ice.

The new ice thickness model was further used to quantify several basic integral quantities related to the ice body geometry of FRIS and its main sub-areas. The results are summerised in Table 4.

	Area (10^3 km^2)	**Ice volume** (meteoric, marine) (10^3 km^3)	**Ice mass** (meteoric, marine) (10^3 Gt)	**Mean ice thickness** (m)
Filchner-Ronne-Schelfeis	**487.3**	**343.9** **(> 314.2 , > 17.6)**	**307.6** **(> 280.7 , > 16.1)**	**706**
Ronne Ice Shelf	332.5	216.1 (199.1 , 17.0)	192.9 (177.4 , 15.5)	650
Filchner-Schelfeis	94.5	83.0 (> 70.3 , > 0.6)	74.6 (> 63.2 , > 0.6)	878
Berkner Island	45.3	34.5	30.9	762
Ice rises, ice rumples (w/o Berkner Island)	15.0	10.3	9.2	

Table 4: Integral quantities related to the ice body geometry of FRIS and its main sub-areas. Computation base is the new ice thickness model which considers the ice front positions from Feb. / Mar. 1986 (Ronne Ice Shelf) and Jan.1986 / Oct. 1987 (Filchner-Schelfeis). Marine ice volumes are calculated from the assumption that all marine ice beneath FRIS is completely consolidated.

Acknowledgements

We thank H. Bennat, C.S.M. Doake, P. Holmlund, C. Mayer, U. Nixdorf, V.S. Pozdeev, U. Schirmer, J. Sievers, and F. Thyssen for providing the basic ice thickness data sets and their valuable contributions to the FRIS ice thickness mapping project. Support from the Alfred-Wegener-Institut für Polar- und Meeresforschung, Bremerhaven, Germany, British Antarctic Survey, Cambridge, UK, Bundesamt für Kartographie und Geodäsie, Frankfurt am Main, Germany, Institut für Geophysik, Universität Münster, Germany, Sevmorgeologija, Sankt Peterburg, Russia, and Department of Physical Geography, Stockholm, Sweden, is gratefully acknowledged. The project has received financial support from the European Science Foundation (grant EIS/96/09).

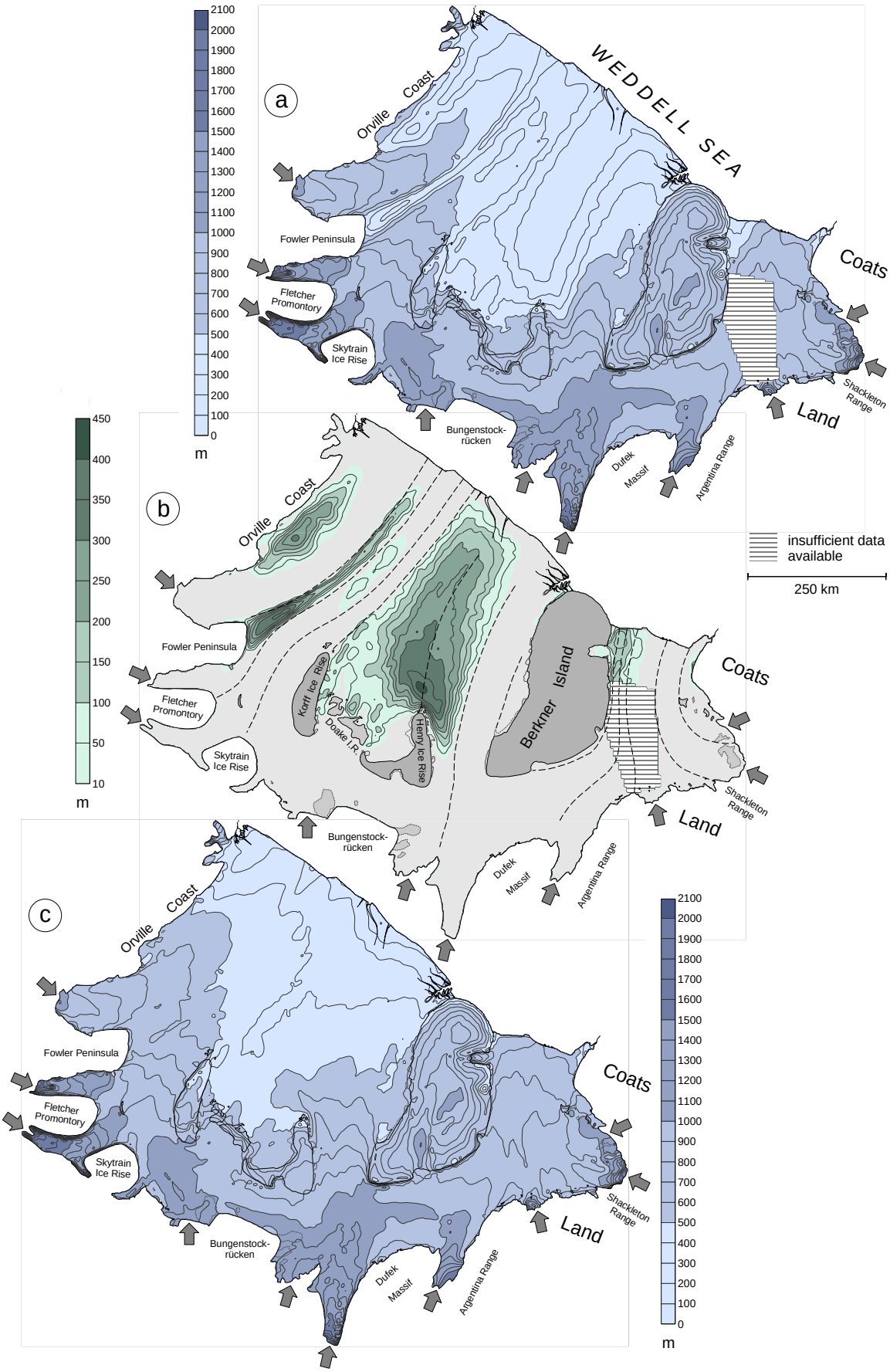

Figure 3: Maps of FRIS showing the distributions of **(a)** meteoric ice thickness, **(b)** basal marine ice layer thickness, and **(c)** total ice thickness. The maps directly derive from the new digital ice thickness model for FRIS. Entrances of main contributory glaciers and ice streams are indicated by arrows. Grounding line, ice front and flowline positions are adopted from Heidrich et al. (1992) and ADD Consortium (2002); the grounding line of Foundation Ice Stream is mapped according to Lambrecht (1998).

References

ADD Consortium (2002). *Antarctic Digital Database, Version 4.0*. SCAR, Cambridge.

Blindow, N. (1994). The central part of the Filchner-Ronne Ice Shelf, Antarctica: internal structures revealed by 40 MHz monopulse RES. *Ann. Glaciol.* **20**, 365-371.

Bombosch, A., and A. Jenkins (1995). Modeling the formation and deposition of frazil ice beneath Filchner-Ronne Ice Shelf. *J. Geophys. Res.* **100**(**C4**), 6983-6992.

Crabtree, R.D., and C.S.M. Doake (1986). Radio-echo investigations of Ronne Ice Shelf. *Ann. Glaciol.* **8**, 37-41.

Engelhardt, H., and J. Determann (1987). Borehole evidence for a thick layer of basal ice in the central Ronne Ice Shelf. *Nature* **327**, 318-319.

Grosfeld, K., H.H. Hellmer, M. Jonas, H. Sandhäger, M. Schulte, and D.G. Vaughan (1998). Marine ice beneath Filchner Ice Shelf: Evidence from a multi-disciplinary approach. In: Jacobs, S.S., and R.F. Weis (eds.), *Ocean, Ice, and Atmosphere: Interactions at the Antarctic Continental Margin, Antarctic Research Series* **75**, AGU, Washington DC, 319-339.

Heidrich, B., J. Sievers, H.W. Schenke, and M. Thiel (1992). Digitale Topographische Datenbank Antarktis – Die Küstenregionen vom westlichen Neuschwabenland bis zum Filchner-Ronne-Schelfeis interpretiert aus Satellitenbilddaten. *Nachrichten aus dem Karten- und Vermessungswesen* **I**(**107**), 127-140.

Hempel. L., and H. Oerter (1995). Airborne radio echo sounding during the Filchner V field season. In: Oerter, H. (ed.), *FRISP Report* **9**, AWI, Bremerhaven, 31-38.

Holmlund, P. (1992). Radio-echo soundings along the lowermost part of the Baileys Ice Stream in the Filchner Ice Shelf Basin. In: Oerter, H. (ed.), *FRISP Report* **6**, AWI, Bremerhaven, 98-100.

Jezek, K., and RAMP Product Team (2002). *RAMP AMM-1 SAR image mosaic of Antarctica*. Fairbanks, AK: Alaska SAR Facility, in association with the National Snow and Ice Data Center, Boulder, CO (digital media).

Johnson, M.R., and A.M. Smith (1997). Seabed topography under the southern and western Ronne Ice Shelf, derived from seismic surveys. *Ant. Science* **9**(**2**), 201-208.

Lambrecht, A. (1998). Investigations on mass balance and dynamics of the Ronne Ice Shelf, Antarctica. *Ber. z. Polarforsch.* **265**, AWI, Bremerhaven, 143 pp (in German).

Lambrecht, A., C. Mayer, L. Hempel, U. Nixdorf, and H. Oerter (1995). Glaciological investigations in the grounding line area of the Foundation Ice Stream, Antarctica. *Polarforsch.* **65**(**1**), 15-25 (published in 1997).

Lambrecht, A., C. Mayer, H. Oeter, and U. Nixdorf (1999). Investigations of the mass balance of the southeastern Ronne Ice Shelf, Antarctica. *Ann. Glaciol.* **29**, 250-254.

Makinson, K. (1996). Hot water drilling on Ronne Ice Shelf 1995/96. In: Oerter, H. (ed.), *FRISP Report* **10**, AWI, Bremerhaven, 55-57.

Mantripp, D.R., J. Sievers, H. Bennat, C.S.M. Doake, K. Heidland, J. Ihde, M. Jonas, B. Riedel, A.V. Robinson, R. Scharroo, H.W. Schenke, U. Schirmer, F. Stefani, D.G. Vaughan, and D.J. Wingham (1996). *Topographic Map (Satellite Image Map) 1:2 000 000 Filchner-Ronne*-Schelfeis, Antarctica. 2nd Edition, Institut für Angewandte Geodäsie, Frankfurt am Main.

Nicholls, K.W., K. Makinson, and A.V. Robinson (1991). Ocean circulation beneath the Ronne ice shelf. *Nature* **354**, 221-223.

Nicholls, K.W., S. Østerhus, K. Makinson, and M.R. Johnson (2001). Oceanographic conditions south of Berkner Island, beneath Filchner-Ronne Ice Shelf, Antarctica. *J. Geophys. Res.* **106**(**C6**), 11,481-11,492.

Oerter, H., C. Drücker, J. Kipfstuhl, U. Nixdorf, and W. Graf (1992a). The Filchner IV campaign and the 320 m deep ice core B15. In: Oerter, H. (ed.), *FRISP Report* **6**, AWI, Bremerhaven, 47-53.

Oerter, H., J. Kipfstuhl, J. Determann, H. Miller, D. Wagenbach, A. Minikin, and W. Graf (1992b). Evidence for basal marine ice in the Filchner-Ronne ice shelf. *Nature* **358**, 399-401.

Pozdeev, V.S., and R.G. Kurinin (1987). New data on ice sheet morphology, bedrock and bottom relief in the Southern Weddell Sea Basin, West Antarctica. *Antarktika; doklady komissii* **26**, 66-71 (in Russian).

Robin, G. de Q., C.S.M. Doake, H. Kohnen, R.D. Crabtree, S.R. Jordan, and D. Möller (1983). Regime of the Filchner-Ronne ice shelves, Antarctica. *Nature* **302**, 582-586.

Robinson, A.V., and K. Makinson (1992). Preliminary results from hot water drilling and oceanographic measurements under Ronne Ice Shelf. In: Oerter, H. (ed.), *FRISP Report* **6**, AWI, Bremerhaven, 40-46.

Sievers, J., C.S.M. Doake, J. Ihde, D.R. Mantripp, V.S. Pozdeev, B. Ritter, H.W. Schenke, F. Thyssen, and D.G. Vaughan (1995). Validating and improving elevation data of a satellite-image map of Filchner-Ronne Ice Shelf, Antarctica, with results from ERS-1. *Ann. Glaciol.* **20**, 347-352.

Thyssen, F. (1988). Special aspects of the central part of Filchner-Ronne Ice Shelf, Antarctica. *Ann. Glaciol.* **11**, 173-179.

Thyssen, F. (1991). Flugprogramm auf dem Filchner-Ronne-Schelfeis und Berkner Island. In: Miller, H., and H. Oerter (eds.), Die Expedition ANTARKTIS-VIII mit FS „Polarstern“ 1989/90, Bericht vom Fahrtabschnitt ANT-VIII/5, *Ber. z. Polarforsch.* **86**, AWI, Bremerhaven, 77-79.

Thyssen, F., A. Bombosch, and H. Sandhäger (1992). Elevation, ice thickness and structure mark maps of the central part of Filchner-Ronne Ice Shelf. *Polarforsch.* **62**(**1**), 17-26 (published in 1993).

Vaughan, D.G. (1990). Preliminary results of British Antarctic Survey fieldwork on Ronne Ice Shelf 1988/89. In: Miller, H. (ed.), *FRISP Report* **4**, AWI, Bremerhaven, 50-51.

Vaughan, D.G., C.S.M. Doake, and D.R. Mantripp (1991). Thematic maps of Filchner-Ronne Ice Shelf. In: Miller, H., and H. Oerter (eds.), *FRISP Report* **5**, AWI, Bremerhaven, 8-11.

Wingham, D.J., C.S.M. Doake, J. Ihde, D.R. Mantripp, R. Scharroo, H.W. Schenke, and J. Sievers (1997). *ESAMCA – Exploitation of satellite altimetry for the monitoring of climate-related change of Antarctic ice shelves.* Final Report to the Commission of the European Communities, DGXII Framework 3 Environment Programme Phase II, Contract EV5C-CT94-0483, Mullard Space Science Laboratory, Holmbury St. Mary, U.K.